Vehicle System Dynamics

International Journal of Vehicle Mechanics and Mobility

ISSN: (Print) (Online) Journal homepage: https://www.tandfonline.com/loi/nvsd20

Suspension parameters design for robust and adaptive lateral stability of high-speed train

Yuan Yao, Xiangwang Chen, Hu Li & Guang Li

VEHICLE SYSTEM DYNAMICS
2023, VOL. 61, NO. 4, 943–967
https://doi.org/10.1080/00423114.2022.2062012

RESEARCH ARTICLE

Suspension parameters design for robust and adaptive lateral stability of high-speed train

Yuan Yao, Xiangwang Chen, Hu Li and Guang Li

State Key Laboratory of Traction Power, Southwest JiaoTong University, Chengdu, People's Republic of China

ABSTRACT

An adequate hunting stability margin is required through the optimisation and matching of bogie suspension parameters for high-speed trains. Moreover, the dynamics design is particularly important for the robust lateral stability to adapt to wheel–rail wear and track deformation. The hunting stability margin of vehicles, as well as the wheel–rail contact state adaptability should be taken into account. In this regard, the robust hunting stability Pareto optimisation of bogie suspension parameters for different wheel–rail wear stages is executed. A method for the centralised optimisation of key bogie suspension parameters based on vehicle lateral robust stability is presented, and the principle of two typical parameters matching for high-speed vehicles is summarised. In addition, in order to make the vehicle automatically adapt to different wheel–rail geometry contact states without any sensors and control systems, a new idea of frequency-dependent stiffness (SDF) of yaw damper is proposed to ensure the lateral stability margin especially in extreme wheel–rail contact states, which is verified through the vehicle linear system stability and ride comfort comparative analysis. Finally, the adaptive stabilisation mechanism of the vehicle with the frequency-dependent stiffness of yaw damper is clarified.

ARTICLE HISTORY

Received 12 October 2021
Revised 2 March 2022
Accepted 6 March 2022

KEYWORDS

High-speed train; robust stability; adaptive stability; suspension parameters design; frequency-dependent stiffness

1. Introduction

During the long-term service, the lateral hunting stability of high-speed trains will be inadequate due to wheel–rail wear and variations in contact states, which could lead to phenomena such as the carbody low-frequency swaying, the bogie high-frequency shaking, even vibration alarm, and so on [1,2]. Main mitigation measures at present consist of shorting the wheel reprofiling interval, grinding rails frequently, and even reducing the speed, which affect the normal safe operation of trains and increase the costs of operation and maintenance [2]. The essence of these phenomena is that the lateral stability of vehicles equipped with passive suspension elements with fixed parameters is inadequate in a wide wheel–rail contact state taking into account higher and lower equivalent conicities. The optimisation and matching of bogie suspension parameters is particularly important for the design of vehicle robust hunting stability to adapt to wheel–rail wear and track

CONTACT Yuan Yao yyuan8848@163.com

deformation. The hunting stability margin of vehicles in long-term service, as well as the adaptability to the track changes should be taken into account in this task.

Although the lateral stability of railway vehicles can be strengthened with the help of advanced mechanisms or active suspension systems [3–8], the optimisation of conventional passive suspension elements still could be considered as one of the efficient methods. Several studies on improving hunting stability of wheel–rail vehicles based on the optimisation of suspension parameters [9–11] and wheel–rail profiles [12–15] have been carried out. In general, the design optimisation of a mechanical system is multidisciplinary and the task is to find effective trade-off solutions for the complicated and conflicting design criteria [16]. In the suspension design of railway vehicles, a compromised design normally gives consideration to lateral stability, curving performance, ride quality, wheel–rail wear and so on. The genetic algorithm is known as one of the most powerful tools in global optimisation and is particularly useful in design optimisation problems of sophisticated nonlinear systems. He et al. [17] proposed a methodology via the genetic algorithm, which can handle the conflicting requirements of rail vehicle design effectively. They also utilised the genetic algorithm to settle the curving performance optimisation problem of a railway vehicle model with 21 DOF. Johnsson et al. [18] optimised passive damping elements of bogie suspension by using the genetic algorithm, and optimised passive damping elements in the bogie suspensions can improve the safety and comfort of the railway vehicle. Bideleh et al. [19] solved the wear/comfort Pareto optimisation problem of bogie suspension by using the GA. A 50 degree-of-freedom railway vehicle model developed has been studied, whose aim is to reduce wheel/rail contact wear and improve passenger ride comfort, and Pareto optimal solutions of design parameters achieved here guarantee wear reduction and comfort improvement for railway vehicles. Uncertainties in the design parameters of suspension systems can negatively influence the dynamics behaviour of railway vehicles. Bideleh et al. [20] analysed the robustness of bogie suspension parameters achieved from the wear/comfort Pareto optimisation problem. Jiang et al. [21] developed a multi-parameter and multi-objective optimisation platform to optimise the curving dynamic performance of an articulated monorail vehicle. At present, most works of the literature focus on the tradeoff between vehicle running performance on tangent track, curving performance and vehicle wear performance for the suspension parameters optimisation of railway vehicles. In fact, due to operating on large curve, the curving performance of high-speed vehicles is not prominent and lateral stability is the focus of the suspension parameters design.

In this regard, the robust hunting stability Pareto optimisation of bogie suspension parameters for different wheel–rail contact geometry is considered. A method for the optimisation of key bogie suspension parameters based on vehicle hunting stability is presented, and the law of parameter optimal matching is summarised. In addition, in order to make the vehicle automatically adapt to different wheel–rail contact states without any sensors and control systems, an innovative idea of frequency-dependent stiffness (SDF) of yaw damper is proposed to ensure the lateral stability margin especially in extreme wheel–rail contact states, which is verified based on the vehicle linear system stability and ride comfort comparative analysis. Finally, the adaptive stability mechanism of frequency-dependent stiffness of yaw damper is clarified.

2. Dynamics model

2.1. The vehicle linear dynamics model

In order to investigate the vehicle hunting stability, a simplified vehicle lateral dynamics model is established, as shown in Figure 1. The model is composed of seven rigid bodies, which are one carbody, two frames, and four wheelsets. The carbody and the frames have lateral, yaw and roll degrees of freedom, and the wheelsets have lateral and yaw degrees of freedom. The primary suspension is between the wheelset and the frame, which is composed of lateral, longitudinal and vertical stiffness. Besides, the primary rotating arm axle box structure is considered in the model. The secondary suspension is between the carbody and the frame, which is composed of lateral, longitudinal and vertical stiffness, damping and anti-roll stiffness. In order to analyse the effects of the series stiffness of oil damper on vehicle stability, the yaw damper and the secondary lateral damper are established based on the Maxwell model that consists of spring and damper in series. The linear stability of the established vehicle model is emphatically analysed in this study, thus the wheel–rail contact geometry is expressed by equivalent conicity, and the wheel–rail tangential force is calculated by Kalker's linear theory. Referring to one type of high-speed EMU in China, the specific parameters of the model are shown in Appendix Table A1. The equation of the system dynamics model is as follows:

$$M\ddot{x}(t) + C\dot{x}(t) + Kx(t) = Q \tag{1}$$

The x is the degree of freedom vector. The matrices M, C, K, and Q are the mass, damping, stiffness and external force components of the system, respectively. Adopting the complex mode method, Equation (1) is recast into the following state-space form:

$$\dot{y}(t) = Ay(t) \tag{2}$$

The modal shapes and linear stability of the vehicle system are obtained by analysing the eigenvectors and eigenvalues of the system matrix A. The ratio of the real part of eigenvalues to the modulus corresponding to the hunting mode regarded as the natural modal damping is defined as the linear stability index, which is represented by ζ. Usually, when the damping value is positive, it indicates that the linear system is stable. In this paper, a smaller value is selected as the optimisation direction, so we can define that the system is stable if ζ is negative.

This study mainly focuses on the key bogie suspension parameters which affect the vehicle hunting stability, such as the primary longitudinal stiffness *kpx*, the damping of yaw damper *csx*, the damping of secondary lateral damper *csy* and the series stiffness of yaw damper *kncsx*, which are chosen as the optimisation parameters to improve the lateral stability for railway vehicles.

2.2. Maxwell viscoelastic model

At present, most of the dampers used in railway vehicles are oil dampers, which form damping force through throttle orifices, thus reducing the system vibration [22]. In the ideal case, the mechanical properties of an oil damper can be described by a damping element. However, in practice, it is necessary to consider the stiffness of oil compression

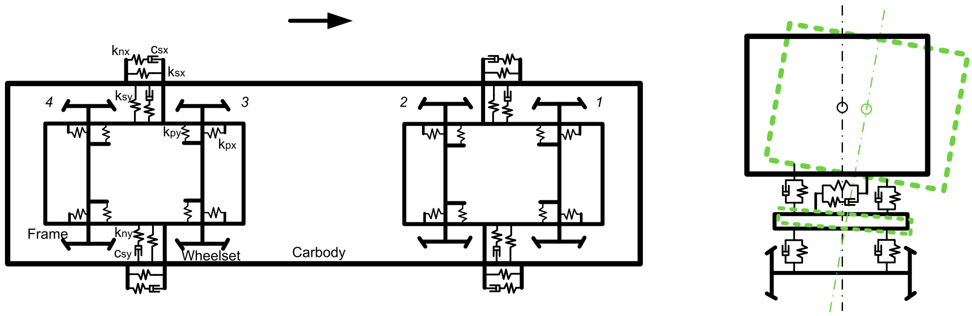

(a) (b)

Figure 1. Simplified vehicle lateral dynamics model.

and valve deformation, as well as series rubber joint deformation. Therefore, it is necessary to introduce a stiffness element, namely a viscoelastic model, to describe the energy storage and consumption characteristics of a damper. According to the test of the yaw damper, the Maxwell equivalent parameter model composed of a damping and a series stiffness element can simulate the dynamic characteristics of the damper in normal working conditions. Compared with the thermal-fluid-structure coupling model, the simplified mechanical model saves the calculation time and is more suitable for the dynamic simulation calculation of high-speed trains. The Maxwell model with damping c and series stiffness k can be expressed as

$$k(x_0 - x) + c\dot{x}_0 = 0 \tag{3}$$

where x and x_0 are the displacements at the end and middle of the model, respectively. According to Laplace transform, the force F of the damper in the complex domain can be obtained as follows:

$$F(\mathrm{s}) = c\dot{x}_0(\mathrm{s}) = \frac{kc}{cs + k}\dot{x}(\mathrm{s}) = \frac{kcs}{cs + k}x(\mathrm{s}) \tag{4}$$

where $s = j\omega$, ω is the circular frequency and j is the imaginary unit.

The equivalent stiffness k_e and equivalent damping c_e between two ends of damper are

$$k_e = \frac{kcs}{cs + k} \tag{5a}$$

$$c_e = \frac{kc}{cs + k} \tag{5b}$$

It can be seen that the equivalent stiffness and equivalent damping are related to the action frequency, they are also known as dynamic stiffness and dynamic damping. The frequency-dependent characteristics are shown in Figure 2 (a,b). At low frequency, the damper mainly reflects the damping characteristic, and the stiffness of the damper can be ignored. With the increase of frequency, the stiffness characteristic of the damper increases, meanwhile, the damping characteristic decreases.

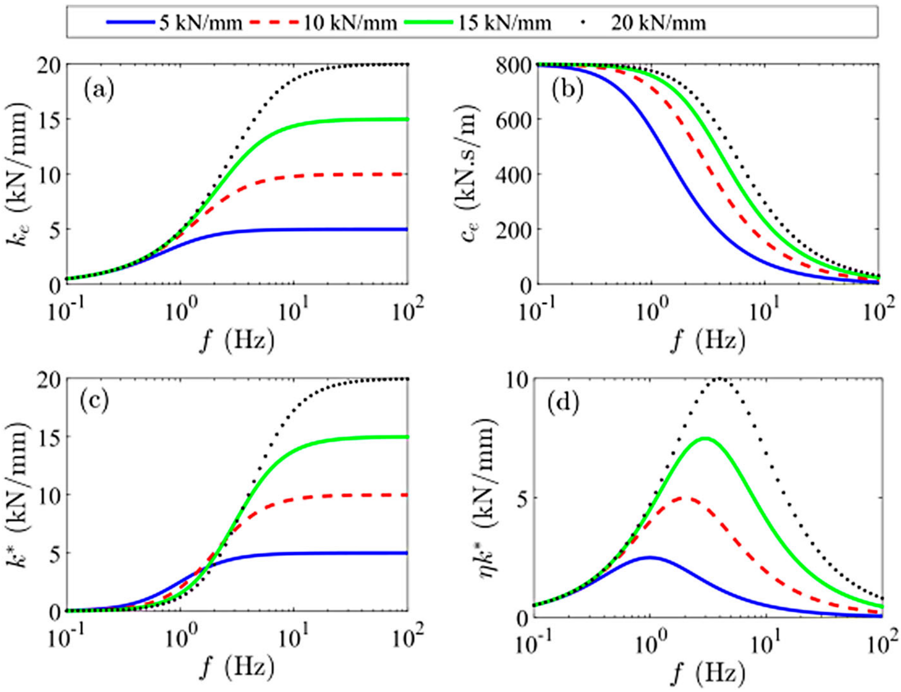

Figure 2. Frequency-dependent characteristics of the Maxwell viscoelastic model with different series stiffness.

Substitute $s = j\omega$ into Equation (5a) to get complex stiffness

$$k_e = (1 + j\eta)k^* \tag{6}$$

where the real part $k^* = kc^2\omega^2/(k^2 + c^2\omega^2)$ is called the storage modulus and the imaginary part $\eta k*$ is called the energy dissipation modulus, meanwhile, $\eta = k/c\omega$ is the dissipation factor and $\phi = \tan^{-1}(\eta)$ is the dissipation angle. The storage modulus and energy dissipation modulus represent the ability of damper storing energy and damping converting mechanical energy into thermal energy, respectively. Their frequency-dependent characteristics are shown in Figure 2 (c,d). With the increase of frequency, the stiffness characteristic becomes obvious and the energy storage effect increases. The energy dissipation effect increases first and then decreases, which means the damper has the optimal energy dissipation condition.

Assuming the end displacement of damper is $x = A\sin\omega t$, the dissipation power W in one cycle is

$$W = \frac{\pi A^2 k^2 c\omega}{c^2\omega^2 + k^2} \tag{7}$$

Let $dW/d\omega = 0$, the optimal dissipation energy condition can be obtained as follows:

$$\omega_{opt} = \frac{k}{c} \tag{8}$$

That is, when the circular frequency ω of the damper is equal to the ratio of series stiffness k to damping c, the energy dissipation power is the largest. At this point, the storage modulus of the damper equals the energy dissipation modulus, and the dissipation factor η is 1, the dissipation angle ϕ is 45°.

3. Robust stability

3.1. Robust stability index

The change of wheel–rail contact geometry caused by rail deformation as well as profile wear of tread and rail will affect the vehicle dynamic performances. According to the operation experience of high-speed trains in China, the phenomena of carbody low-frequency swaying in the state of new tread, as well as the bogie high-frequency shaking in the state of worn tread occur regularly, which is caused by the insufficient lateral stability in extreme wheel–rail contact states. Therefore, a large hunting stability margin in a wide range of wheel–rail contact states is required. That is to say, the trains need strong robustness for varying extensively wheel–rail contact states.

For the vehicle lateral stability, on the one hand, when the wheel–rail contact equivalent conicity is low, such as the state of new reprofiling wheel and new grinding rail profile, the carbody is prone to hunting or called primary hunting, which is characterised by low-frequency lateral swaying of the carbody, and mainly affects ride comfort. On the other hand, the high equivalent conicity after wheel tread wear makes the stability margin of the bogie hunting insufficient, and then the secondary hunting instability occurs, which is manifested as the bogie high-frequency shaking. To describe the lateral stability of trains in two different wheel–rail contact states, the low conicity stability index ζ_{low} corresponding to the equivalent conicity λ of 0.05, and the high conicity stability index ζ_{high} corresponding to the λ of 0.4 are defined respectively. Vehicle lateral riding quality is related to lateral stability, especially in the low conicity condition. Existing studies have found that there is a contradictory relationship between the optimisation of ζ_{low} and ζ_{high} for the suspension with fixed parameters. That is, the better the low conicity stability of the vehicle has, the worse the high conicity stability is, and vice versa [9–11]. In order to evaluate the influence of disturbance resulting from wheel–rail contact geometry on the vehicle hunting stability, the λ is distributed in a certain range, and the stability indexes of the system are calculated with different equivalent conicities, and their standard deviation is defined as the equivalent conicity robustness index, denoted by $std(\zeta_{\lambda})$. The smaller the index value, the smaller the influence of equivalent conicity variation on the system stability. According to the operational experience of the Chinese high-speed railway [23], the $std(\zeta_{\lambda})$ is obtained by analysing the different equivalent conicities uniformly distributed in the range of 0.05–0.4 in this study. The robust stability indexes and corresponding calculation conditions are shown in Table 1. Therefore, the lateral stability optimisation design of bogie suspension parameters is a multi-objective optimisation process.

3.2. Multi-objective optimal

Multi-objective optimisation problems usually have a solution set, which is called the Pareto set, and its image in the objective function space is called the Pareto frontier. The Pareto frontier is the objective values set after optimisation, each point has the advantages that other points do not have, from which we can find the contradiction between the

Table 1. Robust stability indexes for multi-objective optimisation.

	Calculation condition		
Index	v (km/h)	λ	Description
ζ_{low}	250	0.05	Linear stability index in the low conicity condition
ζ_{high}	350	0.40	Linear stability index in the high conicity condition
$std(\zeta_{\lambda})$	350	0.05–0.40	Equivalent conicity robustness index

multiple objectives. According to the different design priorities, we can manually select the optimal solution to meet the performance requirements in the Pareto set. The NSGA-II algorithm [24] can keep the population diversity and improve computational efficiency. Thus, it is an effective algorithm for solving multi-objective optimisation problems. A fast non-dominated sorting genetic algorithm NSGA-II with an elitist strategy is selected for multi-objective optimisation design in this study. Most of the default settings of this algorithm are kept and only two parameters are changed. They are population size and generation number. In this study, the population size is set to 5000, and the number of generation is set to 100.

Four key suspension parameters, including the primary longitudinal stiffness *kpx*, the damping of secondary lateral damper *csy*, the damping of yaw damper *csx*, and the yaw damper series stiffness *kncsx* are optimised. Three optimisation objectives, including the ζ_{low}, ζ_{high}, and $std\ (\zeta_{\lambda})$ are considered. The multi-objective optimal design problem is stated as

$$\min\{\zeta_{low}, \zeta_{high}, std(\zeta_{\lambda})\} \tag{9}$$

4. Parameters design

4.1. Pareto frontier

The Pareto frontier and Pareto set for the parameters are obtained by iteration and updating suspension parameters to optimise the vehicle system performances towards the defined objectives, which are shown in Figure 3. The two coordinate axes represent the vehicle stability index ζ_{low} and ζ_{high} corresponding to the equivalent conicity of 0.05 and 0.4, respectively. The smaller the value, the more stable the system. The colour in the figure indicates the equivalent conicity robustness index $std(\zeta_{\lambda})$. The darker the colour, the better equivalent conicity robustness is. That is, the variation of wheel–rail contact geometry has a minor effect on vehicle stability, indicating a long vehicle tread turning period and strong track adaptability.

The Pareto frontier illustrates the contradiction between optimisation objectives. The system stability can be improved at the expense of the equivalent conicity robustness. Similarly, the ζ_{low} and ζ_{high} are contradictory. Therefore, it is necessary to select the suitable objective values from the Pareto frontier that satisfies the design requirements, and then to acquire the corresponding suspension parameters.

In order to investigate the suspension parameter matching laws which results in different vehicle dynamic performances, four clusters of objectives denoted by letters *A*, *B*, *C* and *D* are selected in different spaces from the optimisation frontier, as shown in Figure 3. Clusters *A*, *B* and *C* indicate that the vehicles equipped with their respective suspension

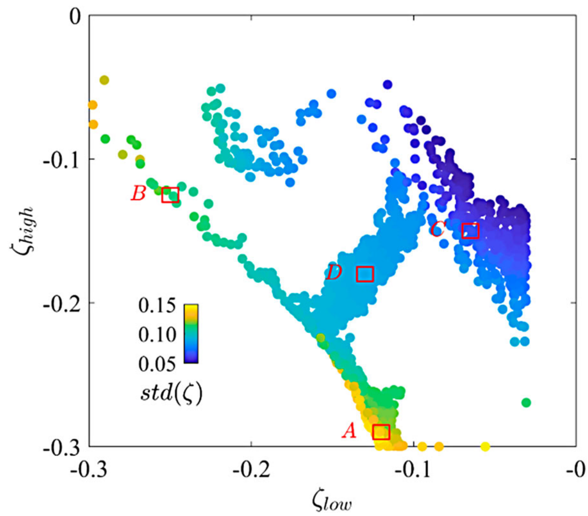

Figure 3. Pareto frontier of multi-objective optimisation (Colour figure online).

parameters have better high conicity stability, low conicity stability and conicity robustness, respectively. However, the performances of other two objectives are compromised. Cluster *D* gives attention to all three objectives, with which the vehicle's performances are balanced.

4.2. Parameters matching mode

Figure 4 reflects the suspension parameter distribution for the selected four clusters in the form of a Box-plot. The emphasised optimisation objective of each cluster is different, and the matching laws of suspension parameters for the corresponding objectives can be obtained by observing the figure.

As can be seen from the figure, the damping values of the yaw damper and secondary lateral damper can be divided into two types. The first one is that the two dampers both adopt larger damping values, such as clusters *A*, *B* and *D*, where the *csx* of 3800 kN.s/m and the *csy* of 50 kN s/m are optimised. And the second one is that both of them adopt smaller damping values, such as cluster *C*, where the *csx* and *csy* are about 500 and 15 kN s/m, respectively. It can be seen that employing the smaller damping values can achieve better equivalent conicity robustness, and the larger damping values are required to obtain a large stability margin. In fact, the two types of the suspension parameter matching mode are in line with the existing high-speed trains in China. In addition, cluster *A* has larger values of *kpx* and *kncsx* compared with cluster *B*, thus achieving favourable high conicity stability, but its low conicity stability is poor. In other words, increasing the longitudinal suspension stiffness improves the secondary hunting stability for the vehicle in the high conicity condition, whereas the decrease of longitudinal stiffness is beneficial to the primary hunting stability for the wheel–rail contact states of low equivalent conicity.

The effects of combined *kpx* and *kncsx* on vehicle system stability are presented in Figure 5. Subfigures (a,b) are contour plots of the linear stability index of the vehicle

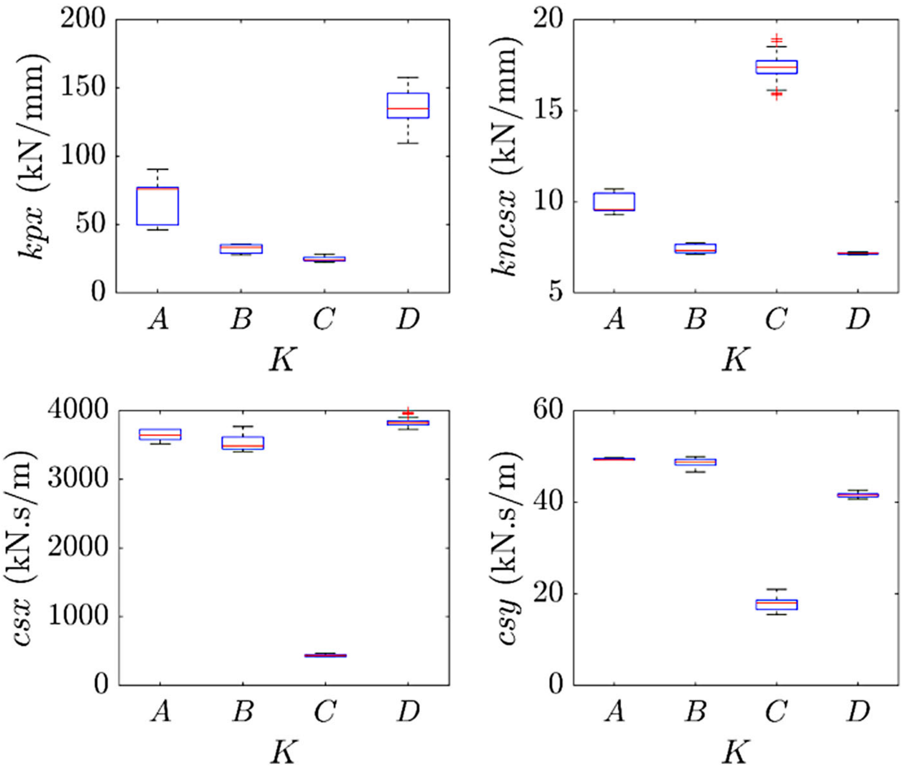

Figure 4. Suspension parameters distribution of the four clusters.

adopting larger and smaller damping values respectively. The scenario is commonly experienced for the vehicle, with a medium equivalent conicity of 0.17 and operating speed of 350 km/h. Both types of suspension parameters allow excellent vehicle stability, and the optimal ranges of *kpx* and *kncsx* are similar. For a specific stability index, such as the contour marked with – 0.3 in subfigure (a), the *kpx* and *kncsx* exhibit a hyperbola-like relationship. The variation of one parameter can be compensated by adjusting the other one so as to obtain the same vehicle stability margin. Although the optimal ranges of *kpx* and *kncsx* differ considerably for clusters *C* and *D*, it is predictable that adjusting the two parameters simultaneously can still achieve the same dynamic performance. This means that there is no unique matching law for these two longitudinal stiffnesses due to their complementary relationship. If one of the longitudinal stiffnesses is fixed, then the requirements of different performances for the other can be summarised more clearly.

4.3. Factor analysis

It can be drawn from Figure 4 that the optimal damping of the yaw damper has a strong correlation with the secondary lateral damping, from which two modes of suspension parameter matching can be summarised. In order to analyse the influence of other suspension parameters on the optimal damping distribution of the yaw damper, such as the longitudinal stiffness and secondary lateral damping, the optimal values of yaw damping

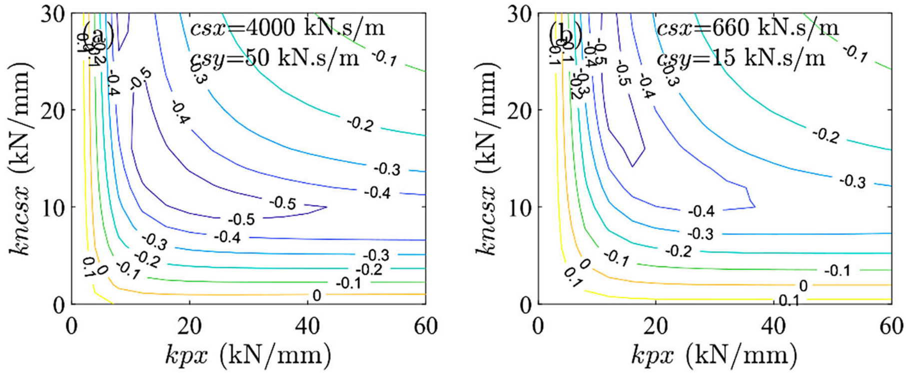

Figure 5. Matching law about the longitudinal stiffness of *kpx* and *kncsx*.

and its series stiffness are calculated for different primary longitudinal stiffnesses and secondary lateral damping. Taking into account the high and low conicity stability indexes, the optimal damping and series stiffness of the yaw damper are obtained with the aid of multi-objective optimisation.

First of all, the effects of *kpx* on the optimal solution distribution of *csx* and *kncsx* are investigated, the range of *kpx* is set to 10–120 kN/mm. In Figure 6(a,b) show the Pareto sets when *csy* is 50 and 15 kN s/m, respectively. The three coordinate axes represent respectively *kpx*, stability index ζ_{low} or ζ_{high}, and optimisation parameter for the yaw damper. It can be seen that the value of *kpx* has little effect on the optimal solution distribution of *csx*. When *csy* is 50 kN s/m, the optimal solution of *csx* is large and approaches the upper optimisation limit no matter which value *kpx* is set to. However, the optimal solution of *csx* is about 600 kN s/m when *csy* is 15 kN s/m. The value of *kpx* has a certain influence on the optimal solution distribution of *kncsx*, as *kpx* decreases, the corresponding optimal value of *kncsx* increases. The effect of *kncsx* reflected in the figure on vehicle stability is consistent with the above description. Increasing *kncsx* has an adverse effect on the low conicity stability of the vehicle, but the high conicity stability can be improved in this way.

Similarly, the optimal parameters of the yaw damper can be analysed with the variation range of *kpy* as 3–15 kN/mm. The Pareto sets are obtained according to the *csy* of 50 and 15 kN s/m, respectively. It is similar to the analytical results of primary longitudinal stiffness *kpx* that the value of *kpy* has no obvious influence on the optimal parameters of the yaw damper. The analysis indicates that *csy* plays a key role, which determines the optimal damping of the yaw damper. Therefore, much attention should be paid to the matching law between the damping of the yaw damper and secondary lateral damping.

5. Stability analysis

5.1. Linear stability index

In order to analyse the hunting stability of the vehicle with four groups of suspension parameters from the clusters shown in Figure 4, the linear stability index ζ of the vehicle with the variation of equivalent conicity and operating speed is calculated as shown in

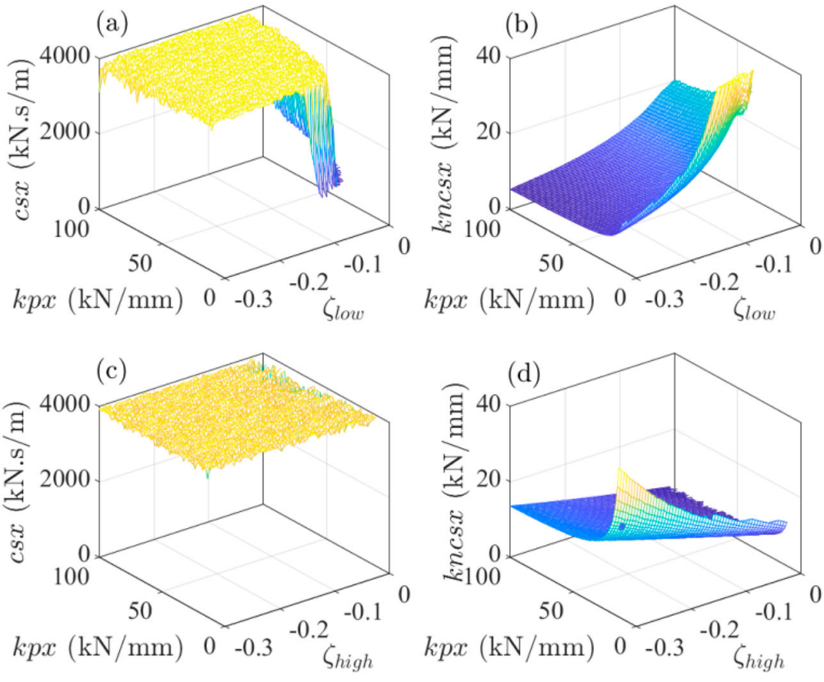

(a). The *csy* is 50 kN.s/m

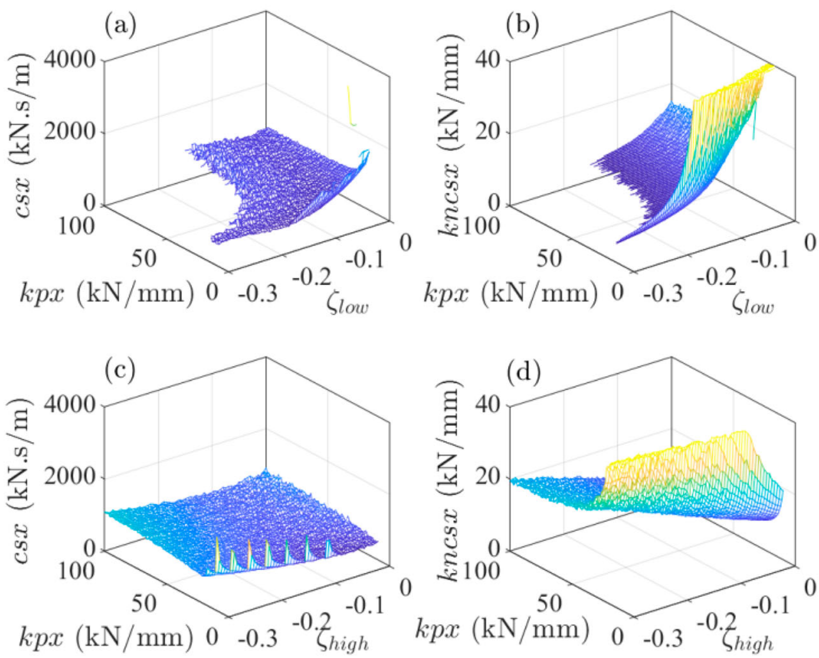

(b). The *csy* is 15 kN.s/m

Figure 6. Optimal parameters of *csx* and *kncsx*.

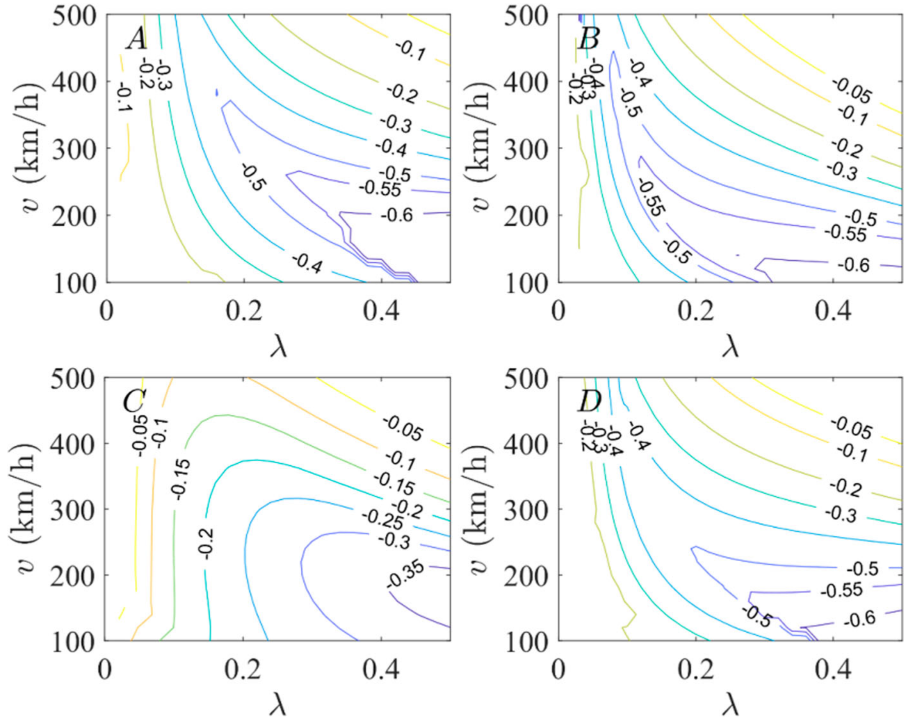

Figure 7. Linear stability indexes of vehicle with the four clusters of suspension parameters.

Figure 7. It can be observed that the speed has little effect on the system stability if the variation of ζ along the longitudinal axis is small, which suggests that the system has strong speed robustness. The influence of the operating speed on the system stability in the low equivalent conicity condition is smaller than that in the high equivalent conicity condition. If the ζ changes little along the horizontal axis, the equivalent conicity robustness $std(\zeta_\lambda)$ of the vehicle is better. It can be drawn from the figure that adopting different suspension parameters has significant effects on the system stability with the variation of equivalent conicity and operating speed.

For clusters *A*, *B* and *D*, the stability margin is larger than cluster *C*, and the stability of cluster *B* is better in the low equivalent conicity condition, while cluster *A* is better in the high equivalent conicity and high-speed condition. However, the system stability of cluster *C* is less affected by the variation of vehicle speed and equivalent conicity. When the vehicle adopts the suspension parameters of cluster *C*, the stability of vehicle with low wheel–rail contact conicity is poor and a larger initial equivalent conicity for tread is needed to ensure the hunting stability in the new tread state. No matter which type of suspension parameter is adopted, the system stability becomes worse if the equivalent conicity of wheel–rail contact is too small. With the increase in operating speed and equivalent conicity, the variation of vehicle stability corresponding to the four clusters of suspension parameters is inconsistent, so it can be inferred that the bifurcation forms of the vehicle non-linear stability will be different.

5.2. Root locus

The root loci of the vehicle linear system with the change of operating speed according to the four groups of suspension parameters on behalf of the four clusters are shown in Figure 8(a), in which the equivalent conicity is 0.1. Each root locus is composed of 25 sets of eigenvalues in the speed range of 20–500 km/h, and each '+' indicates a corresponding mode. A larger symbol represents a larger operating speed. The horizontal axis indicates the mode damping ratio ζ (negative sign indicates stable mode). The vertical axis indicates the damped vibration frequency. The green circle in the figure indicates the maximum hunting mode damping ratio ζ_{max} at this speed, which affects the system stability. Normally, as the speed increases, the hunting-related mode's damping reduces. When the ζ_{max} is greater than 0, the hunting instability occurs. Mostly, the low-frequency hunting mode (1–10 Hz) determines the vehicle hunting critical speed.

Comparing the speed root locus of the vehicle system with the four groups of suspension parameters, it can be found that the root locus curve is consistent with the mode classification of suspension parameters. The first defined as *Type* 1 adopts a larger *csx* and *csy*, such as the suspension parameters according to the clusters *A*, *B* and *D*. The stability of the hunting mode with frequency below 2 Hz is enhanced with the increasing operating speed. Meanwhile, the stability of high-frequency hunting mode reduces with the increasing operating speed, which determines the critical speed of the linear system. The second defined as *Type* 2 adopts the opposite law that a small *csy* is matched with a small *csx*, with which the single hunting mode affects the system stability. The stability decreases with the increase in the operating speed, such as cluster *C*.

The root loci of the vehicle system with the change of wheel–rail contact equivalent conicity are shown in Figure 8(b), in which the operating speed is 350 km/h. Each root locus curve is composed of 25 sets of eigenvalues with the equivalent conicity from 0.02 to 0.5, and each 'o' indicates a corresponding mode. A larger symbol represents a larger equivalent conicity. The red circle in the figure indicates the maximum hunting mode damping ratio ζ_{max} at this equivalent conicity, which determines the system stability margin. Normally, as the equivalent conicity increases, the vehicle hunting stability increases first and then decreases. In the figure, if the normal equivalent conicity λ of the vehicle is located at the turning position of the hunting root locus, the stability varies little with the λ, which indicates that the hunting stability is insensitive to the variation of the λ. In other words, the vehicle has strong adaptability to the geometry variation of wheel–rail contact, which is caused by the variable rail cant and gauge, as well as the wear of rail and tread profile, and others. It is observed that the stability of vehicle equipped with the suspension parameters of *Type* 2 is less affected by the variation of the equivalent conicity. However, the stability margin is worse than the vehicle with the suspension parameters of *Type* 1 in the low equivalent conicity condition. In fact, the vehicle hunting instability due to the low wheel–rail contact equivalent conicity occurs occasionally, especially in the situation of wheel re-profiling and rail grinding. Therefore, the vehicle with the suspension parameters of *Type* 2 needs to match a large conicity tread to avoid carbody large-amplitude swaying due to the poor low conicity stability.

For the suspension parameters of *Type* 1, the root locus of vehicle hunting mode consists of two curves connected end to end, which can achieve better low conicity stability. Compared with cluster *A*, the stiffness parameters of *kpx* and *kncsx* in cluster *B* are smaller, and

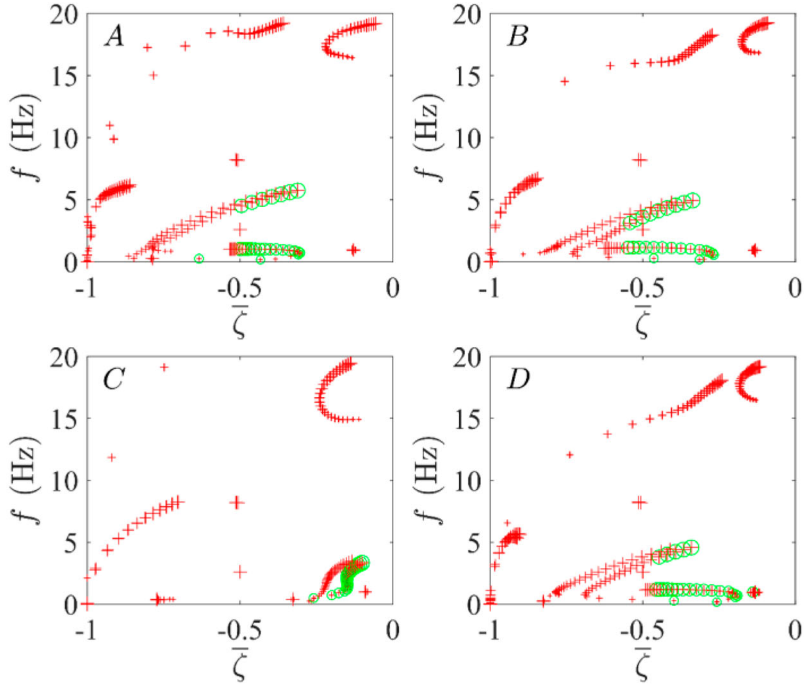

(a). The speed varies from 20 to 500 km/h

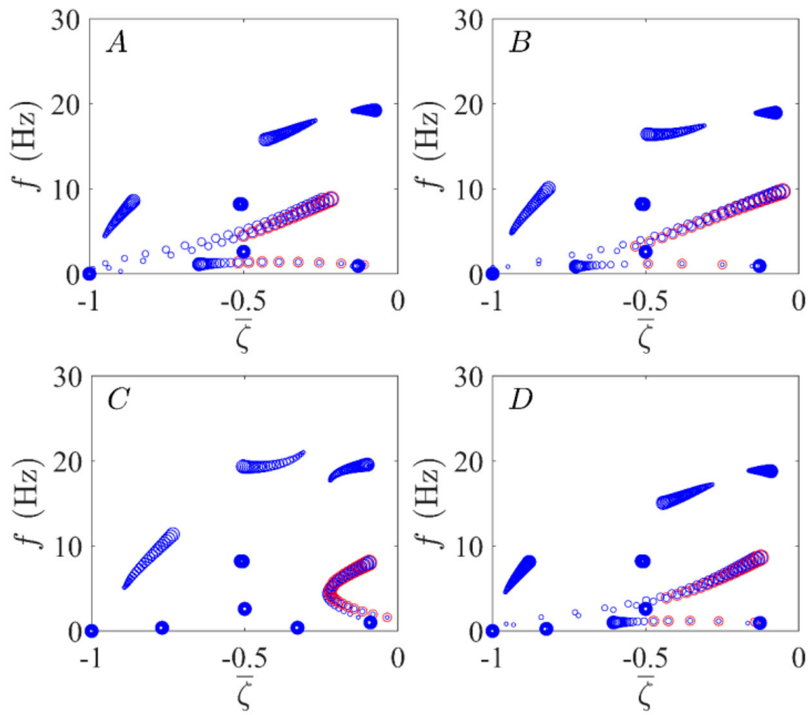

(b). Equivalent conicity varies from 0.04 to 0.5

Figure 8. Root loci of vehicle with the four clusters of suspension parameters (Colour figure online).

its low conicity stability is better but the high conicity stability is worse. In the condition of low equivalent conicity, the low-frequency hunting mode (called primary hunting) of the carbody determines the system stability. On the contrary, the high-frequency hunting mode (called secondary hunting) of the bogie determines the system stability in the high equivalent conicity condition. With the increase of the operating speed or the equivalent conicity, the vehicle instability mode suddenly changes from the low-frequency primary hunting to the high-frequency secondary hunting, which corresponds to the subcritical bifurcation in vehicle nonlinear dynamics.

For the suspension parameters of *Type* 2, the root locus of vehicle hunting mode is a 'C' shaped curve. The damping ratio of the hunting mode varies less than *Type* 1 with the changes in the operating speed and the equivalent conicity, such as the cluster *C*. Similarly, in the conditions of low equivalent conicity and high equivalent conicity, the stability of low-frequency primary hunting and high-frequency secondary hunting is worse, and the system stability can be achieved better in the condition of middle equivalent conicity. Different from *Type* 1, the system stability is determined by the hunting mode with a single root locus, that is, with the increase of speed or equivalent conicity, the instability mode gradually evolves from the low-frequency primary hunting to the high-frequency secondary hunting. There is no hunting frequency transition, which corresponds to the supercritical bifurcation in vehicle nonlinear dynamics.

5.3. Nonlinear bifurcation

In order to analyse the influence of the suspension parameter matching mode on the vehicle's nonlinear bifurcation characteristics, the nonlinear bifurcation characteristics of vehicles with new tread and worn tread are studied [25,26]. The railway vehicle is a typical nonlinear dynamic system, which is mainly reflected in the nonlinear characteristics of the wheel–rail contact relationship and the suspension elements. The nonlinearity of wheel–rail contact includes the contact geometry and the saturation of creep force. In this study, a nonlinear vehicle lateral dynamics model is established, and the nonlinear bifurcation of the vehicle hunting adopting the four groups of suspension parameters is analysed using a direct integral method. The nonlinear characteristics of wheel–rail contact geometry and creep saturation are considered in the dynamics model. Based on the linear dynamics model described above, two kinds of nonlinear equivalent conicity curves produced by new tread and worn tread with negative slope are considered respectively. The wheel–rail contact equivalent conicity is a nonlinear function of wheelset lateral displacement, which is expressed by a polynomial as described in [27]. The equivalent conicity of the new tread and the worn tread is 0.12 and 0.3 at the lateral displacement of 3 mm, respectively. Shen's method [28] is adopted to calculate the wheel–rail nonlinear creep force.

The vehicle hunting bifurcation can be obtained using the direct integration of the nonlinear model with a group of changed initial values, which are approximate periodic solutions and were calculated by numerical integration. In the bifurcation diagram, the state set of all DOF corresponding to the approximate periodic solution at different positions is taken as the initial value for numerical integration. With this approach, the unstable periodic solution can be found by scanning point by point. Figure 9 shows the bifurcation curves of the wheelset lateral displacement versus the operating speed. The blue

Table 2. Two types of suspension parameters.

Type	*kpx* (kN/mm)	*kpy* (kN/mm)	*csy* (kN s/m)	*csx* (kN s/m)	*kncsx* (SDF) K1	K2 (kN s/m)	K3 (kN s/m)
1	50	5	50	4000	1.5	8	6
2	50	5	15	660	1.5	10	2

solid points in the figure represent the stable limit cycles, and the red hollow points represent the unstable limit cycles. For the worn tread, the wheelset lateral displacement has a typical supercritical bifurcation according to the four groups of suspension parameters, which is caused by the negative slope of the equivalent conicity function. The corresponding speed of a point where its vertical coordinate equals 0 is known as the linear critical speed, and the minimum speed of the unstable limit cycle is the nonlinear critical speed. The linear critical speed corresponding to the four groups of suspension parameters is proportional to the linear stability index calculated in Figure 8.

However, for the new tread, the subcritical bifurcation occurs for the vehicle with *Type* 1 suspension parameters. Compared with cluster *B*, cluster *A* has higher linear and nonlinear critical speeds due to its better linear stability in conditions of high equivalent conicity and high speed. The bifurcation type of cluster *C* with large damper damping is the supercritical bifurcation, and its linear critical speed is lower than the nonlinear critical speed.

Based on the analyses of the root loci and contour plots, as well as the bifurcation characteristics of nonlinear dynamics, two types of vehicle hunting characteristics can be concluded. The large hunting stability margin always contradicts the hunting stability robustness. That is, the suspension parameters can be designed to make the vehicle have a large stability margin, especially in the condition of low conicity, but at the expense of equivalent conicity robustness and the risk of instability mode transition. On the other hand, the suspension parameters can be matched to improve the robustness of stability in normal wheel–rail contact, and even to reduce the depth of tread wear, but with a poor stability margin especially in extreme wheel–rail contact states.

6. Adaptive stability

6.1. Frequency-dependent stiffness requirements

The system linear stability index ζ corresponding to the combination of *csx* and *kncsx* is calculated in different operating speeds v and equivalent conicities λ. The two types of suspension parameters are shown in Table 2 according to the two parameter modes concluded above. All parameters in the model for comparison are the same except for the *csy*, *csx* and *kncsx*. The results are shown in Figure 10. The horizontal axis is the variable *kncsx* and the vertical axis is the variable *csx*. Each subfigure in the figure represents the contour of the linear stability index ζ. The deeper the colour, the smaller the stability index, and the better the vehicle lateral stability. In the figure, the virtual line represents the parameter matching relationship between *csx* and *kncsx* at different action frequencies where they meet the optimal dissipation condition from Equation (8).

Figure 10(a–c) are the results of *Type* 1. The equivalent conicity λ from left to right is 0.05, 0.17 and 0.4, respectively. Considering that it is prone to hunting instability in the

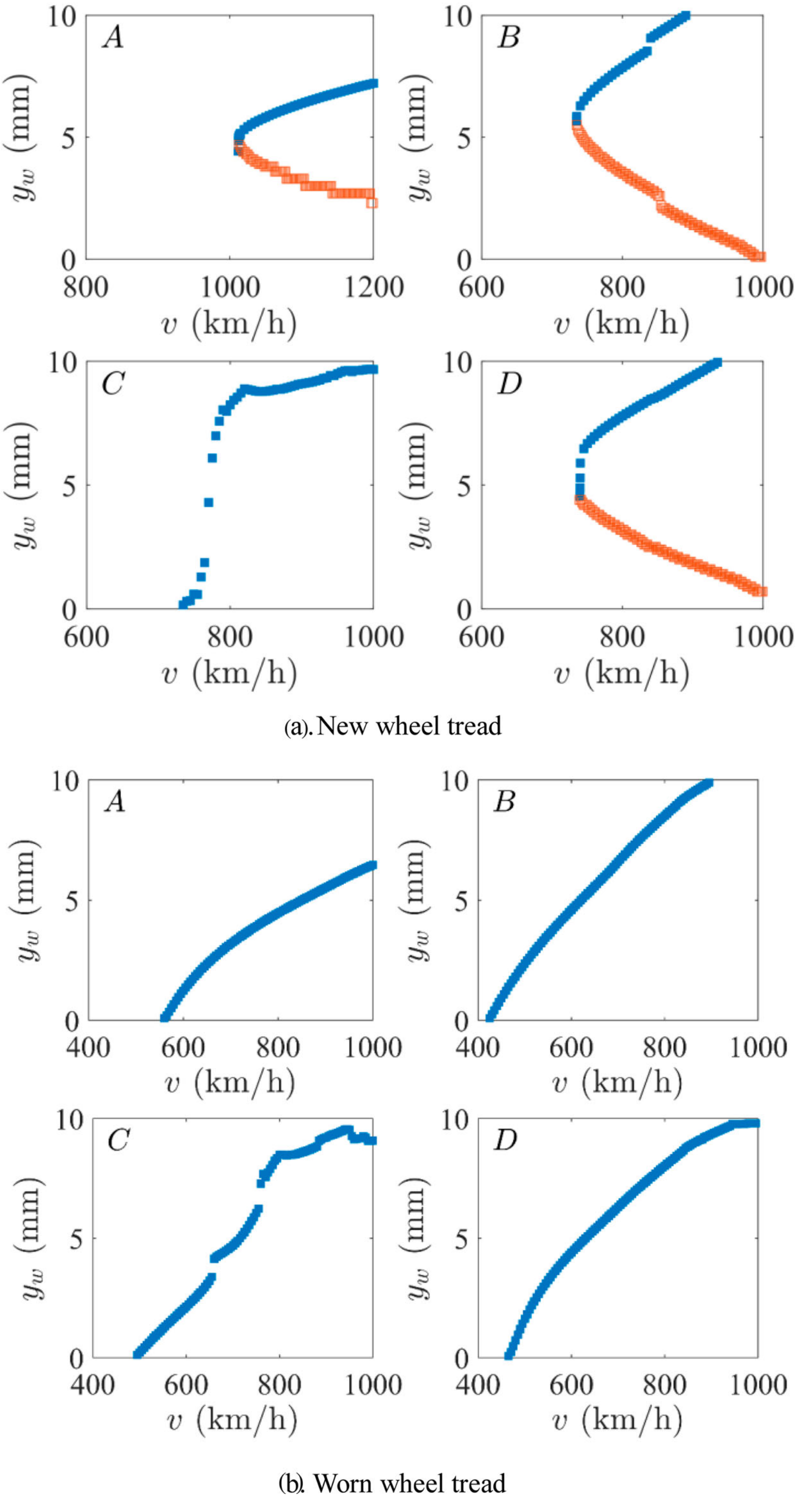

Figure 9. Bifurcation characteristics of vehicle with the four clusters of suspension parameters (Colour figure online).

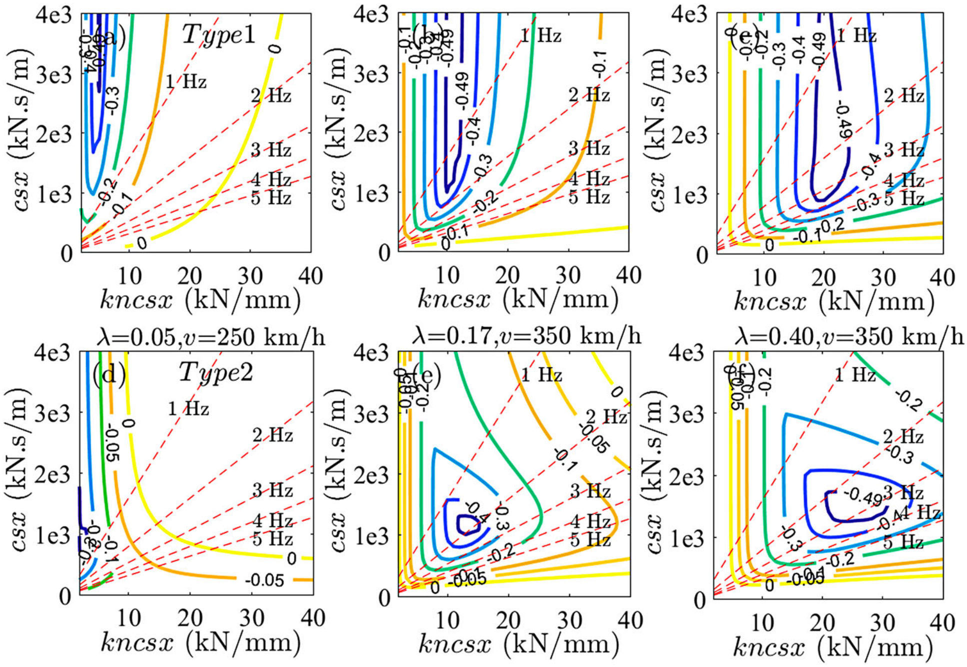

Figure 10. Optimal of *csx* and *kncsx* in different operating conditions.

conditions of low speed and low conicity, the calculation speed v of the first conicity condition is 250 km/h, and the latter two conditions are 350 km/h. It can be seen from the figure that with the increase of equivalent conicity, the series stiffness *kncsx* needs to be increased to improve the vehicle hunting stability margin. The optimal value of *csx* is about 500–1500 kN s/m, and the optimal *csx* increases with the increase of equivalent conicity. The optimal parameters *kncsx* and *csx* of yaw damper generally meet the optimal dissipation condition from Equation (8). That is, the ratio of the optimal *kncsx* to *csx* is close to the circular frequency of vehicle hunting. The vehicle hunting frequency increases with the λ and v, so the corresponding optimal ratio of *kncsx* to *csx* needs to be increased. Subfigures (d–f) show the results of *Type* 2, similar conclusions can be drawn from them.

In short, the optimal series stiffness of the yaw damper is related to the wheel–rail contact equivalent conicity and operating speed, namely the corresponding hunting frequency. The optimal stiffness decreases with the decrease of hunting frequency, especially in the low wheel–rail contact conicity condition, a smaller series stiffness is required. On the contrary, a larger stiffness is required for high conicity. The selection of fixed series stiffness needs to compromise the contradiction between the high conicity stability and the low conicity stability, so it cannot guarantee vehicle stability in extreme wheel–rail contact conditions. The yaw damper with frequency-dependent stiffness (SDF) adopts a small series stiffness to guarantee the stability of vehicle in the condition of low equivalent conicity. With the increase of the equivalent conicity, the stiffness of the yaw damper increases with the increase of hunting frequency, which can improve the lateral stability of the vehicle in the condition of high equivalent conicity.

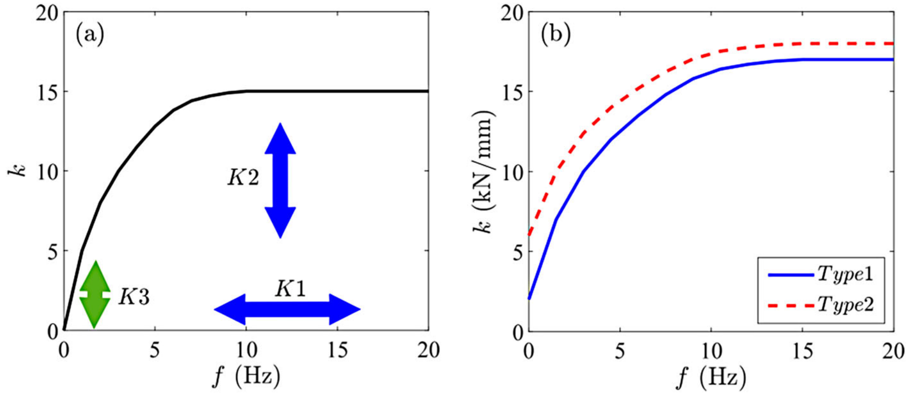

Figure 11. The SDF of yaw damper for the two types of suspension parameters.

6.2. Optimisation of SDF

The characteristic curve shape of frequency-dependent series stiffness of yaw damper can be adjusted through three coefficients as shown in Figure 11(a). From the self-defined standard curve, the abscissa and ordinate are multiplied by the coefficient of $K1$ and $K2$ respectively for scaling. The smaller $K1$ and the larger $K2$, the more obvious the stiffness value changes with frequency. $K3$ represents the static stiffness value. Considering the structure feasibility and actual demand, the optimised curves for the two types of suspension parameters are shown in Figure 11(b), and the specific values of $K1$, $K2$ and $K3$ are listed in Table 2. Hydraulic rubber joints or bushings, which are maturely applied to the automobile industry and other fields, have liquid cavities and damping channels inside. They can realise the dynamic characteristic about low stiffness at low frequency and high stiffness at high frequency with the help of the damping function of liquid channels. Besides, employing the special valve structure inside the damper is an effective way to achieve frequency-dependent stiffness or damping, such as the FSS and FSD damper produced by KONI.

6.3. Lateral dynamic performances comparison

In order to evaluate the application effects of the yaw damper with frequency-dependent stiffness for high-speed trains, the system stability of the two types of vehicles in different wheel–rail contact conicity conditions is investigated. The linear analysis of the system is carried out for the frequency-dependent stiffness model, iterating along the curve of frequency-dependent stiffness allows for finding the stable system vibration frequency and series stiffness value. The root locus and the linear stability index of the two types of vehicles with the equivalent conicity from 0.02 to 0.6 are drawn as shown in Figure 12. A larger symbol in the figure represents a larger equivalent conicity λ. The eigenvalues of the vibration modes related to vehicle hunting within the frequency range of less than 10 Hz are mainly analysed. For *Type* 1 vehicle, the lateral stability in the high conicity condition is significantly improved after frequency-dependent stiffness is implemented. And the stability of *Type* 2 can be improved in both low and high equivalent conicity conditions with the help of frequency-dependent stiffness. It can be seen from the comparison that the yaw

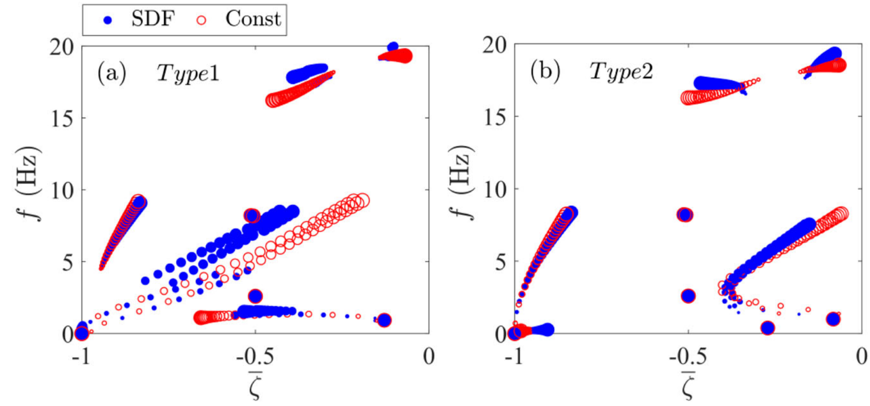

(a).Conicity root locus

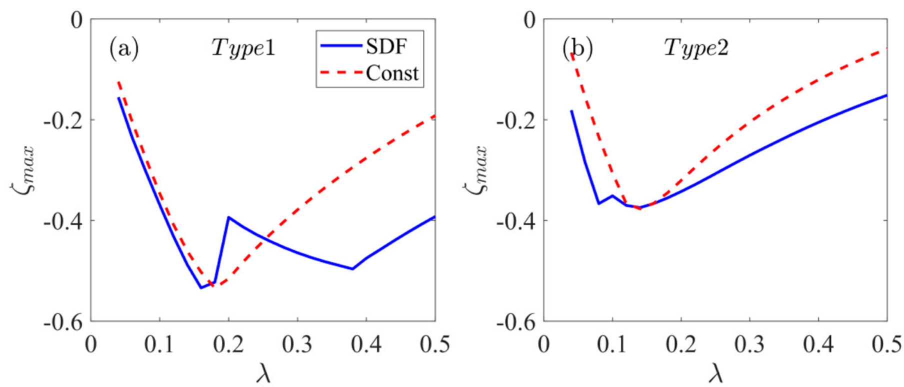

(b). Stability index

Figure 12. Linear stability of vehicle with SDF vs. const stiffness of yaw damper.

damper with frequency-dependent stiffness can remarkably improve vehicle lateral stability, especially in extreme wheel–rail contact conditions, with which the risk of carbody low-frequency swaying and bogie high-frequency shaking can be suppressed.

The improvement of lateral riding quality after using the yaw damper with frequency-dependent stiffness is investigated. In this study, The Wuhan-Guangzhou high-speed railway track lateral irregularity spectrum with the frequency range from 0.3 to 30 Hz is used as the track input, the frequency response function of lateral vibration of carbody subjected to random track irregularities is obtained with the aid of the pseudo-excitation method [29,30], using the frequency response function one can get the pseudo-displacement response and the corresponding power spectral density, through which the riding quality index of carbody is calculated. The calculation of the riding quality index in the frequency domain has the advantage of fast calculation, which is conducive to the multi-objective and multi-parameter optimisation analysis of vehicle suspension parameters.

The calculation results of the riding quality index are shown in Figure 13. The lateral riding quality of carbody is strongly correlated to the vehicle's lateral stability. Therefore,

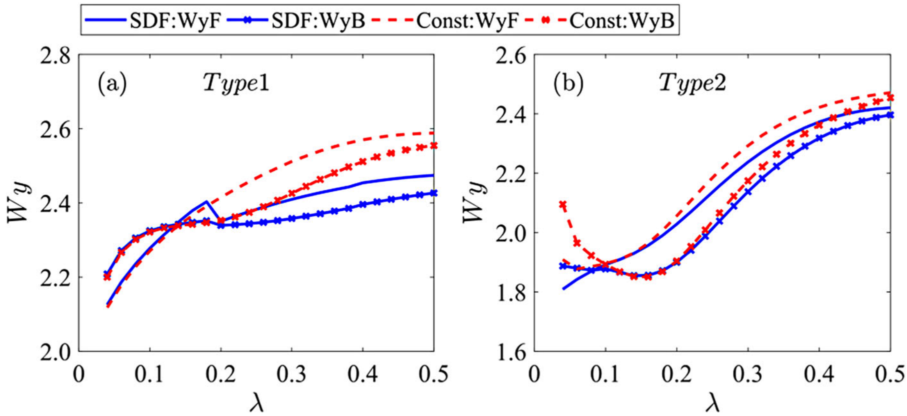

Figure 13. Lateral ride index of carbody with SDF vs. const stiffness of yaw damper.

the improvement of lateral riding quality by employing the yaw damper with frequency-dependent stiffness is similar to the analytical results of lateral stability. Using the yaw damper with frequency-dependent stiffness is able to enhance the lateral riding quality of *Type* 1 vehicle in the high conicity condition. While for *Type* 2 vehicle, the lateral riding quality shows some improvement under both low and high conicity conditions.

6.4. Adaptive stability mechanism

The vehicle hunting frequency increases with the operating speed and wheel–rail contact equivalent conicity, and the lateral stability is poor in the low-frequency and high-frequency domains. The mechanism can be explained according to the modal energy analysis of vehicle hunting. The hunting energy of the carbody and bogie under different operating speed and equivalent conicity conditions is shown in Figure 14. The dark red symbol in the figure indicates that the hunting energy of the carbody accounts for 100%. On the contrary, the blue part indicates that the hunting energy of bogies is relatively high. If the hunting frequency is close to the natural frequency of carbody suspension, the resonance occurs and the hunting energy of carbody is large. The system stability and ride comfort are prone to deteriorate, which is called primary hunting instability. With the increase in hunting frequency, vehicle stability is improved but then becomes worse again. When the hunting frequency increases to a certain extent, the high-frequency hunting instability occurs, it is called secondary hunting instability. The former exhibits the carbody low-frequency swaying, and the latter is the bogie high-frequency shaking phenomenon.

According to the hunting energy proportion of vehicle in different frequency ranges, as well as the parameter optimisation laws of the yaw damper, the mechanism of the stiffness of yaw damper for high-speed trains can be summarised. If the equivalent conicity of wheel–rail contact is low, the hunting energy of carbody accounts for the main part, and a smaller stiffness of the yaw damper can reduce the yaw motion coupling between the carbody and the bogie, which is conducive to the system stability and reducing the carbody swaying. When the secondary hunting instability occurs, the main energy originates from the bogie hunting, and the stiffness effect of the yaw damper strengthens the motion coupling thus suppressing the bogie hunting through the relatively static carbody. The hunting

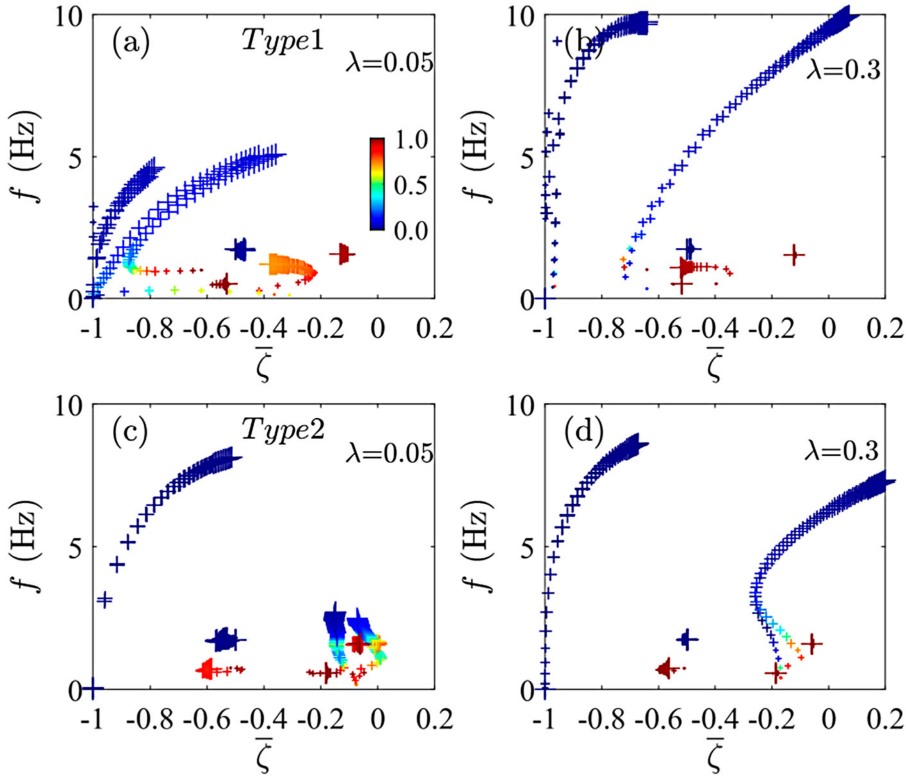

Figure 14. Modal energy distribution of carbody and bogie (Colour figure online).

energy of the bogie increases with the increase in equivalent conicity and operating speed, therefore, the corresponding optimal stiffness of the yaw damper needs to be increased. In short, the frequency-dependent stiffness joints overcome the shortage of dynamic stiffness ratio of the traditional yaw damper with fixed parameters. Employing the new yaw damper with a large dynamic stiffness ratio is beneficial to the lateral stability of the vehicle in a wide wheel–rail contact states.

7. Conclusion

(1) In order to reasonably design the vehicle suspension parameters and ensure the lateral dynamic performances of high-speed trains in the whole service cycle. The robust hunting stability Pareto optimisation of bogie suspension parameters for different wheel–rail wear stages is executed. A method for the centralised optimisation of key suspension parameters, including the primary longitudinal stiffness, the damping of yaw damper, secondary lateral damper and the series stiffness of yaw damper is presented. In this way, two types of suspension parameter matching modes are summarised. The first mode adopts larger damping values of yaw damper and secondary lateral damper to achieve an adequate stability margin, while the second mode utilises small damping of the two types of damper for stability robustness to the varied wheel–rail contact states. Both of them need to carefully optimise the longitudinal

stiffness of the primary suspension and the series stiffness of the yaw damper to compromise the contradiction between the vehicle stability in the high conicity and low conicity contact conditions.

(2) In addition to dissipating the vehicle hunting energy through the damping of the yaw damper, the stiffness effect is more critical to vehicle hunting stability. A small stiffness is conducive to improving the carbody hunting stability of vehicle in the low conicity contact condition. On the contrary, a large stiffness enhances the coupling between the carbody and bogie yaw motion, which is beneficial to suppress the bogie hunting in the high conicity condition, thus reducing the risk of bogie high-frequency shaking. The dynamic stiffness ratio of the yaw damper with fixed parameters hardly fulfils the requirement of vehicles in wide wheel–rail contact states. For this contradiction, the concept of frequency-dependent stiffness (SDF) for the yaw damper is proposed to ensure the lateral stability margin especially in extreme wheel–rail contact states, which are verified based on the comparative analysis of vehicle linear system stability and ride comfort. Employing the yaw damper with frequency-dependent stiffness joints in series evidently improves the vehicle's lateral stability adaptively in abnormal wheel–rail contact conditions, thus extending the tread reprofiling and rail grinding intervals, to reduce the maintenance cost of high-speed trains operation.

Disclosure statement

No potential conflict of interest was reported by the author(s).

Funding

The material in this paper is based on work supported by grants (51735012) from the National Natural Science Foundation of China, National Railway Group Science and Technology Program grant (N2020J026, N2021J028), and Traction Power State Key Laboratory grant (2022TPL_Q02) of the Independent Research and Development Projects.

References

[1] Zhai WM, Liu PF, Lin JH, et al. Experimental investigation on vibration behaviour of a CRH train at speed of 350 km/h. Int J Rail Transp. 2015;3(1):1–16.
[2] Li GD. Wheel-rail contact relation improvement and running adaptability for high speed emu. [PhD thesis]. Southwest Jiaotong University; 2019 (in Chinese) .
[3] Fu B, Giossi RL, Persson R, et al. Active suspension in railway vehicles: a literature survey. Railway Eng Sci. 2020;28(1):3–35.
[4] Yao Y, Li G, Sardahi Y, et al. Stability enhancement of a high-speed train bogie using active mass inertial actuators. Veh Syst Dyn. 2019;57(3):389–407.
[5] Allotta B, Pugi L, Colla V, et al. Design and optimization of a semi-active suspension system for railway applications. J Mod Transp. 2011;19(4):223–232.
[6] Wei XK, Zhu M, Jia LM. A semi-active control suspension system for railway vehicles with magnetorheological fluid dampers. Veh Syst Dyn. 2016;54(7):982–1003.
[7] Jiang JZ, Matamoros-Sanchez AZ, Zolotas A, et al. Passive suspensions for ride quality improvement of two-axle railway vehicles. Proc Inst Mech Eng Part F: J Rail and Rapid Transit. 2015;229(3):315–329.
[8] Lewis TD, Jiang JZ, Neild SA, et al. Using an inerter-based suspension to improve both passenger comfort and track wear in railway vehicles. Veh Syst Dyn. 2020;58(3):472–493.
[9] Yao Y, Li G, Wu GS, et al. Suspension parameters optimum of high-speed train bogie for hunting stability robustness. Int J Rail Transp. 2020;8(3):195–214.

[10] Chen XW, Yao Y, Shen LJ, et al. Multi-objective optimization of high-speed train suspension parameters for improving hunting stability. Int J Rail Transp. 2021. doi:10.1080/23248378.2021.1904444.
[11] Li G, Wu RD, Deng XX, et al. Suspension parameters matching of high-speed locomotive based on stability/comfort pareto optimization. Veh Syst Dyn. 2021. doi:10.1080/00423114.2021.1979602.
[12] Qi YY, Dai HY, Wu PB, et al. RSFT-RBF-PSO: a railway wheel profile optimisation procedure and its application to a metro vehicle. Veh Syst Dyn. 2021. doi:10.1080/00423114.2021.1955135.
[13] Ye YG, Qi YY, Shi DC, et al. Rotary-scaling fine-tuning (RSFT) method for optimizing railway wheel profiles and its application to a locomotive. Railway Eng Sci. 2020;28(2):160–183.
[14] Jahed H, Farshi B, Eshraghi MA, et al. A numerical optimization technique for design of wheel profiles. Wear. 2008;264(1-2):1–10.
[15] Persson I, Iwnicki SD. Optimisation of railway profiles using a genetic algorithm. Veh Syst Dyn. 2004;41(suppl):517–527.
[16] Mohebbi M, Rezvani MA. Multi objective optimization of aerodynamic design of high speed railway windbreaks using lattice Boltzmann method and wind tunnel test results. Int J Rail Transp. 2018;6(3):183–201.
[17] He Y, McPhee J. Optimization of the lateral stability of rail vehicles. Veh Syst Dyn. 2002;38(5):361–390.
[18] Johnsson A, Berbyuk V, Enelund M. Pareto optimisation of railway bogie suspension damping to enhance safety and comfort. Veh Syst Dyn. 2012;50(9):1379–1407.
[19] Bideleh SMM, Berbyuk V, Persson R. Wear/comfort Pareto optimisation of bogie suspension. Veh Syst Dyn. 2016;54(8):1053–1076.
[20] Bideleh SMM. Robustness analysis of bogie suspension components Pareto optimised values. Veh Syst Dyn. 2017;55(8):1189–1205.
[21] Jiang Y, Wu P, Zeng J, et al. Multi-parameter and multi-objective optimisation of articulated monorail vehicle system dynamics using genetic algorithm. Veh Syst Dyn. 2020;58(1):74–91.
[22] Gao HX, Chi MR, Jin XS, et al. Study on the non-linear parametric model of hydraulic dampers before relieving for railway vehicles.). 26th symposium of the international association of vehicle system dynamics. 2019 Aug. 12–16; Gothenburg, Sweden.
[23] Shi HL, Wang JB, Wu PB, et al. Field measurements of the evolution of wheel wear and vehicle dynamics for high-speed trains. Veh Syst Dyn. 2018;56(8):1187–1206.
[24] Deb K, Pratap A, Agarwal S, et al. A fast and elitist multi-objective genetic algorithm: NSGA-II. IEEE Trans Evol Comput. 2002;6(2):182–197.
[25] Dong H, Zhao B, Deng YY. Instability phenomenon associated with two typical high speed railway vehicles. Int J Non-Linear Mech. 2018;105:130–145.
[26] Dong H, Wang QS. On the critical speed: supercritical bifurcation, and stability problems of certain type of high-speed rail vehicle. Shock Vib. 2017. 2017: 1–9.
[27] Yao Y, Wu GS, Sardahi Y, et al. Hunting stability analysis of high-speed train bogie under the frame lateral vibration active control. Veh Syst Dyn. 2018;56(2):297–318.
[28] Iwnicki S. Handbook of railway vehicle dynamics. Boca Raton: CRC/Taylor & Francis; 2006.
[29] Lin JH. Virtual excitation method of random vibration. Beijing: Science Press; 2004 (in Chinese).
[30] Liu XX, Zhang YH, Guo HF, et al. Random vibration analysis procedure of railway vehicle. Veh Syst Dyn. 2019;58(12):1873–1892.

Appendix

Table A1. The vehicle model parameters.

Symbol	Definition	Value
m_w	Mass of the wheelset	1639 kg
I_w	Yaw inertia of the wheelset	822 kg m^2
m_f	Mass of bogie frame	2328 kg
I_{fx}	Roll inertia of bogie frame	2110 kg m^2
I_{fz}	Yaw inertia of bogie frame	4080 kg m^2
m_c	Mass of carbody	38936 kg
I_{cx}	Roll inertia of carbody	1.67e6 kg m^2
I_{cy}	Yaw inertia of carbody	9.61e5 kg m^2
m_m	Mass of motor	750 kg
m_{cx}	Mass of yaw damper	20 kg
kpz	Primary vertical stiffness per axle	0.75 kN/mm
ksx	Secondary longitudinal stiffness	0.133 kN/mm
ksy	Secondary lateral stiffness	0.133 kN/mm
ksz	Secondary vertical stiffness	0.2 kN/mm
csz	Secondary vertical damper damping	10 kN s/m
cpz	Primary vertical damper damping	10 kN s/m
k_ϕ	Stiffness of anti-roll torsion bar	4.15 MN m/rad
$2l_1$	Lateral spacing of primary suspension	2000 mm
l_b	Length of axle box arm	480 mm
$2b$	Wheel base	2500 mm
$2L$	Length between bogie centers	17,375 mm
$2l_0$	Distance of the contact spot	1493 mm
$2l_2$	Lateral spacing of the secondary suspension	2200 mm
$2l_{cx}$	Lateral spacing of yaw damper	2700 mm
r_0	The wheel rolling radius	460 mm
f_ξ	The longitudinal creep coefficient	1e7 N
f_η	The lateral creep coefficient	1e7 N
k_r	The contact stiffness of the wheel–rail	500 kN/mm
λ_e	Wheel–rail contact conicity	0.05, 0.40
v	Operating speed	350 km/h
kpx	Primary longitudinal stiffness	*Optimised*
kpy	Primary lateral stiffness	*Optimised*
csy	Secondary lateral damper damping	*Optimised*
$kncsx$	Series stiffness of yaw damper damping	*Optimised*
csx	Yaw damper damping	*Optimised*